CNN-based Aerosol Particle Classification Using 2D Representations of Single-Particle Mass Spectrometer Data

Guanzhong Wang
Institute for Applied Physics and Measurement Technology
University of the Bundeswehr Munich
Neubiberg, Germany
guanzhong.wang@unibw.de
ORCID: 0009-0000-8144-1892

Heinrich Ruser
Institute for Applied Physics and Measurement Technology
University of the Bundeswehr Munich
Neubiberg, Germany
heinrich.ruser@unibw.de
ORCID: 0000-0001-6929-3276

Julian Schade
Institute of Chemistry and Environmental Engineering
University of the Bundeswehr Munich
Neubiberg, Germany
julian.schade@unibw.de
ORCID: 0000-0002-7906-6744

Johannes Passig
Joint Mass Spectrometry Centre
University of Rostock
Rostock, Germany
johannes.passig@uni-rostock.de
ORCID: 0000-0002-3876-1716

Ralf Zimmermann
Joint Mass Spectrometry Centre
University of Rostock
Rostock, Germany
ralf.zimmermann@uni-rostock.de

Günther Dollinger
Institute for Applied Physics and Measurement Technology
University of the Bundeswehr Munich
Neubiberg, Germany
guenther.dollinger@unibw.de

Thomas Adam
Institute of Chemistry and Environmental Engineering
University of the Bundeswehr Munich
Neubiberg, Germany
thomas.adam@unibw.de

Abstract—Single-particle mass spectrometry (SPMS) is a powerful real-time measurement technique to analyze the chemical composition of atmospheric aerosol particles: individual particles are desorbed and ionized to generate a bipolar mass spectrum that expresses the particle's chemical composition, giving clues to its origin and atmospheric processes. Popular approaches to classify SPMS data rely on clustering algorithms, resulting in the inability to achieve automated classification. Here, we present a modified deep learning approach for automatic classification of SPMS data in real-time. Before being processed by a convolutional neural network (CNN), the one-dimensional (1D) mass spectrum is converted into a two-dimensional (2D) representation, since in 2D, global and local features of the spectra are extracted more efficiently. Trained on real-world aerosol mass spectra from a month-long field measurement campaign, the proposed 2D-CNN model achieves a high mean classification accuracy of 92%, outperforming several well-known algorithms based on 2D-CNN, as well as a recently proposed 1D-CNN algorithm trained using 1D representations of mass spectra.

Keywords—CNN, aerosol particle, single-particle mass spectrometry, real-time air quality monitoring

I. INTRODUCTION

Aerosol particles are one of the main culprits of air pollution and health hazards. Regular monitoring of aerosols is limited to particulate matter (PM) concentrations in the air in specific areas, neglecting the particles' chemical composition. As numerous studies revealed (e.g. [1], [2]), chemical compositions of aerosol particles can have severe effects on human health. Among other techniques to analyze
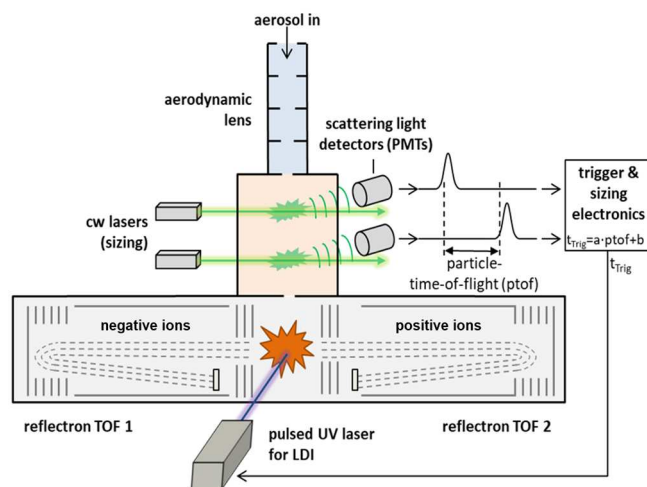

Fig. 1. Working principle of a single-particle mass spectrometer. For details, see [5], [21].

PM, single-particle mass spectrometry (SPMS) stands out as a sensitive measurement technique capable of analyzing the chemical composition of individual airborne aerosol particles in real-time [3]–[5]. The SPMS instrument (see Fig. 1), its working principle, and parameters have been described in detail previously [6], [7]. Briefly, the incoming particles are singled out by an aerodynamic lens, sized via light scattering (using a pair of green cw-lasers (wavelength 532 nm), ellipsoidal mirrors and photomultipliers) before being exposed to a triggered UV laser pulse for laser desorption/ionization (LDI). For each detected particle, the laser trigger time t_{Trig} is calculated as $t_{Trig} = a \cdot ptof + b$,
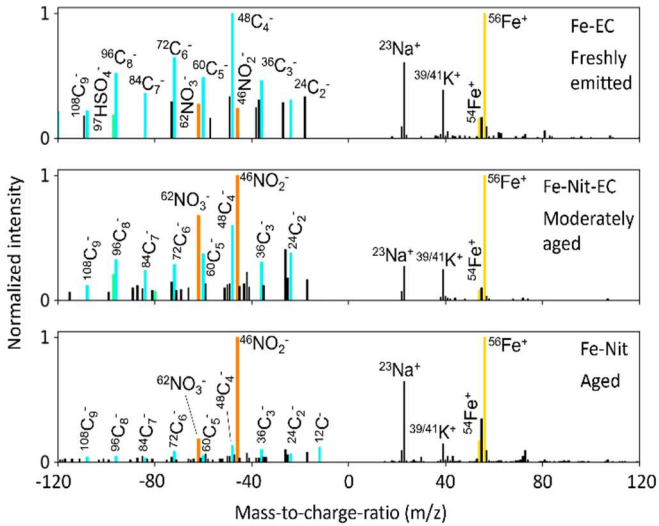
Fig. 2. Several representative bipolar normalized mass spectra as intensities as a function of the mass-to-charge-ratio (m/z) of ions of aerosol particles from ship emissions, with different degrees of atmospheric aging. The positive and negative mass spectra are normalized separately according to their highest ion peaks.

where *ptof* represents the particle-time-of-flight between the two light scattering detectors, *a* denotes a trigger delay parameter and *b* a time offset depending on the instrument alignment. The parameters *a* and *b* are set by the operator during instrument calibration to ensure a high probability of a particle being ionized [8], [9]. After desorption and ionization, anions and cations are separated and detected in a bipolar Time-of-Flight mass spectrometer (TOF-MS). The generated bipolar mass spectrum represents the chemical composition of a single particle, i.e. the intensity distribution of the mass-to-charge ratios (m/z) of the anions and cations. The particle's probable emission source can be assessed by analyzing the specific peak patterns in the mass spectrum.

Aerosol particles may retain their chemical composition even after a long travelling distance in the air. With the SPMS technology, metal components in aerosol particles from ship emissions were detected more than 10 km away from the emission source [7], [10]–[12] with the measurements unaffected by the background aerosols at the local sampling site. Different characteristic ion combinations reveal the degree of aging of the particles, giving estimations of the rough distance to the emission source [7].

The mass spectra used in this work were selected for the purpose of investigating the composition and plausible remote sources of aerosol particles after long-distance transport in air, particularly those emitted from ships. Fig. 2 shows several normalized mass spectra of particles from ships emissions of different degrees of aging, i.e. distances from the source. Mass spectra showing $^{54/56}Fe^+$ ions are typical signatures of particles emitted from ships. Therefore, their positive mass spectra have almost identical patterns. The different combinations of negative signals reflect the particles' degree of aging. For example, the signals of elemental carbon (EC: $^{12n}C^-$) and sulfate ($^{97}[HSO_4]^-$) are stronger in freshly emitted particles and become progressively weaker as the particles are transported in the air, while the signal for nitrate ($^{46}[NO_2]^-$, $^{62}[NO_3]^-$) becomes stronger.

II. CLASSIFICATION APPROACHES

For the classification of SPMS mass spectra, clustering algorithms such as K-means [13], [14] and ART-2a [15], [16] are frequently used. These unsupervised machine-learning (ML) algorithms, operating on unlabeled data, largely rely on manual post-processing to select and merge characteristic clusters based on the calculated cluster centers. This manual processing causes the classification of aerosol particles – analyzed by the SPMS instrument in real-time on-site – to be later performed offline, which prevents the potential for rapid online profiling.

Only very few studies have been published that use supervised ML methods to classify SPMS data automatically, such as Random Forest [17], Support Vector Machines [18] and Multilayer Perceptron [18]. These methods, however, are comparatively constrained in defining characteristic features of mass spectra. In order to reliably distinguish between similar spectra like those displayed in Fig. 2, more sophisticated deep-learning algorithms are needed. Convolutional neural networks (CNNs) offer an attractive alternative to extract characteristic features in the data self-dependently during training, and have been successfully used for two-dimensional (2D) image recognition and classification tasks [19], [20].

CNNs are based on pattern convolutions and designed to operate on 2D data. In a previous study, we treated the 1D mass spectra as 2D "images" of height 1, and adopted a 1D-CNN architecture to convolve patterns during training only in one (length) dimension [21]. To the best of our knowledge, it was the first time that CNNs were proposed for the analysis of SPMS data. Such "skewed" 1D-CNN architecture, however, does not exploit the full potential of 2D convolutions and instead will compromise the understanding of the global information in the mass spectra, due to a small convolution kernel and uni-directional convolution. Consequently, feature relationships between far ends of the spectra are prone to be lost. When distinguishing mass spectra, we need to consider not only the local neighboring ion peaks, but also the global ion composition. In order to allow a 2D-CNN architecture to capture both the local and global pieces of information in the spectra more comprehensively and effectively, we transformed the 1D mass spectra into a 2D matrix by serpentine layout, condensing the information inherit in the "long" 1D spectra within smaller areas (see section III.B). As a consequence, the CNN convolves the 2D representation of the mass spectrum in both length and height directions, allowing to extract the local and global pattern information in the mass spectrum in a more balanced way. In this work, the 2D representation of the mass spectrum to be used as input to a 2D-CNN architecture is validated to demonstrate the superior performance compared to the preciously applied 1D-CNN architecture performing only unidirectional convolution operations.

III. METHODOLOGY

A. Dataset description

In this study, we used mass spectra from a 34-day field measurement campaign (July 1 to August 3, 2022) with a SPMS instrument (manufactured by Photonion, Inc., Germany) located near the port of the German city of Rostock,

TABLE I. OVERVIEW OF THE 13 PREDEFINED PARTICLE CLASSES IN THE LABELED DATASET. POSSIBLE SOURCES AND ION MARKERS OF PARTICLES ARE SUMMARIZED FROM THE LITERATURE AND EXPERT EXPERIENCE. (# MEANS THE NUMBER OF SAMPLES).

| No.	Class	Source	Ion markers	#
1	Elemental carbon (EC)	traffic emissions [14], [15]	$\textbf{\textit{EC}}$: $^{12}C^{\pm}$, $^{24}C_2^{\pm}$, ..., $^{120}C_{10}^{\pm}$	816
2	Organic and elemental carbon (OC-EC)	biomass burning [14], [15]	$\textbf{\textit{OC}}$: $^{27}[C_2H_3]^+$, $^{37}[C_3H]^+$, $^{39}[C_3H_3]^+$, $^{43}[C_4H_7]^+$, $^{51}[C_4H_3]^+$, $^{63}[C_5H_3]^+$, etc; $\textbf{\textit{EC}}$	3383
3	K-rich	biomass burning [14], [15]	$^{39/41}K^+$	3300
4	Ca-rich	lubricating oil of ship engines [7], [15]	$^{40}Ca^+$, $^{56}[CaO]^+$, $^{57}[CaOH]^+$, $^{112}[CaO]_2^+$	3238
5	V-rich	ship fuel emissions [7], [22]	$^{51}V^+$, $^{67}[VO]^+$; $^{54/56}Fe^+$; $^{60}Ni^+$	943
6	Mn-rich	industrial emissions [13]	$^{55}Mn^+$	2904
7	Fe-EC	ship fuel emissions [7], [22]–[26]	$\textbf{\textit{Fe}}$: $^{54/56}Fe^+$, $^{73}[FeOH]^+$; $\textbf{\textit{EC}}$	3306
8	Fe-Nit	ship fuel emissions [7], [22]–[26]	$\textbf{\textit{Fe}}$; $\textbf{\textit{Nitrate}}$: $^{46}[NO_2]^-$, $^{62}[NO_3]^-$	3050
9	Fe-Sul-Nit	ship fuel emissions [7], [22]–[26]	$\textbf{\textit{Fe}}$; $\textbf{\textit{Sulfate}}$: $^{80}[SO_3]^-$, $^{96}[SO_4]^-$, $^{97}[HSO_4]^-$; $\textbf{\textit{Nitrate}}$	2992
10	Fe-Nit-EC	ship fuel emissions [7], [22]–[26]	$\textbf{\textit{Fe}}$; $\textbf{\textit{Nitrate}}$; $\textbf{\textit{EC}}$	3451
11	Fe-dominant	ship fuel emissions [7], [22]–[26]	$\textbf{\textit{Fe}}$; negative signals are empty or very weak	3423
12	Sea salt	sea salt [15], [22]	$\textbf{\textit{Salt}}$: $^{23}Na^{\pm}$, $^{39}[NaO]^+$, $^{62}[Na_2O]^+$, $^{63}[Na_2OH]^+$, $^{35/37}Cl^-$; $\textbf{\textit{Sulfate}}$; $\textbf{\textit{Nitrate}}$	3300
13	Salt-Fe	mixed state [22]	$\textbf{\textit{Fe}}$; $\textbf{\textit{Salt}}$	3300
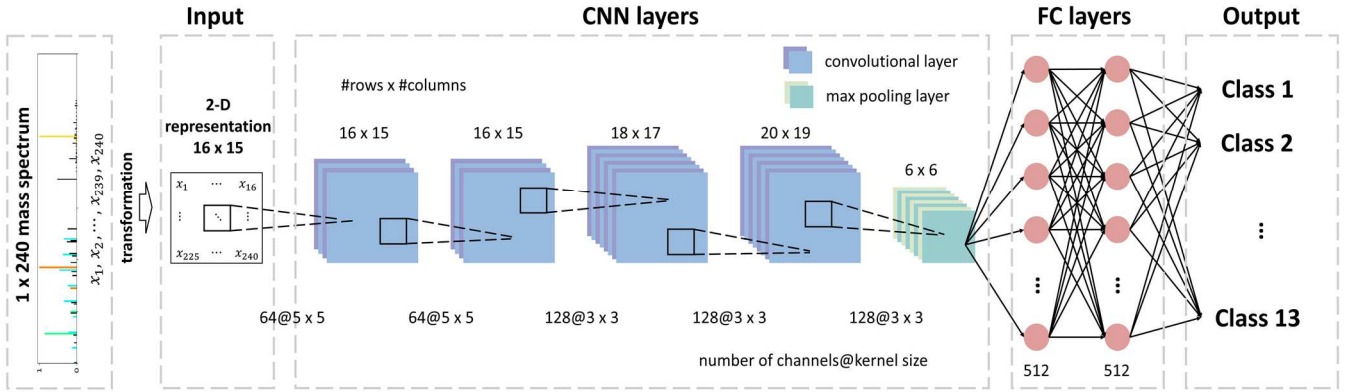
Fig. 3. Architecture of the proposed CNN, comprising 4 convolutional layers, 2 fully connected layers (FC) and 13 outputs (class assignments). The hyperparameters of the network where found by a comprehensive grid search.

at the Baltic Sea coastline (54°10'14.8"N, 12°06'24.7"E, ~7 m above the sea level, ~1.5 km north of the port, close to main shipping lanes). For this study, the recorded bipolar mass spectra were confined to mass-to-charge ratios *m/z* ranging from -120 to +120, and normalized to the maximum intensity of the positive and negative mass spectra, respectively.

To train the classification model, from the measured particle mass spectra we selected and labeled 37,406 spectra as belonging to one of 13 predefined classes, representing the most abundant aerosol particle classes in the atmosphere during the measurement period at the specific sampling location. When labelling, we generally determined a spectrum's class based on the highest ion peaks in both positive and negative mass spectra, together with characteristic combinations of other occurring ions. As this study focuses on particles emitted from ship engines, we appointed the particles to one of five subclasses of transit metals, taking into account the degree of aging (i.e. emission

source distance). In contrast, particles from other sources were not divided into subclasses. Table I lists the 13 different particle classes, their possible sources, the most important ion markers for labelling and the number of spectra in each class in the labeled dataset.

B. Proposed network architecture

In order to bring the SPMS data into 2D representation as input to the CNN network, we converted each normalized mass spectral vector $X = [x_1, ..., x_{240}]$ representing the ion intensities at *m/z* ranging from -120 to +120 excluding 0) into a $m \times n$ 2D matrix representation by vertical stacking, where *m* is the number of rows, *n* is the number columns and $m \times n = 240$, see (1).

$$[x_1, x_2, \cdots x_{m \times n-1}, x_{m \times n}] \rightarrow \begin{bmatrix} x_1 & \cdots & x_n \\ \vdots & \ddots & \vdots \\ x_{n \times (m-1)+1} & \cdots & x_{m \times n} \end{bmatrix} (1)$$

We used a grid search strategy to find the best 2D representation (there are many possible combinations with $m \times n = 240$) and also to optimize the network architecture and its model hyperparameters. After comprehensive search and testing, a 16×15 matrix as input gave the best results in terms of classification accuracy (see Section IV).

Fig. 3 shows the proposed 2D-CNN architecture for the classification of aerosol particles. Four convolutional layers are used to extract and learn the features from the 2D-represented mass spectra of the training dataset, being a fraction of the labeled dataset of spectra, see Section IV. Following the convolutional layers, we applied one Max Pooling layer for downsampling to reduce the dimension of the data that will be fed into two fully connected (FC) layers for classification. For the training of the network we utilized cross-entropy as loss function to compute the difference between the predicted and true values, and minimized that difference with a Adam optimizer. The optimal learning rate was set by grid search to start at 0.0001 and decrease by 10% every 100 epochs, for a total of 300 epochs. The batch size was set to 2048. Moreover, batch normalization and dropout techniques were used during the training process in order to avoid overfitting.

IV. RESULTS AND DISCUSSION

To validate the classification performance, we divided the dataset described in section III.A into two parts (80:20) that do not overlap with each other. That is, 80% of the data were used for training and the remaining 20% were used to test the trained model. Due to the fact that the labeled dataset (roughly 37,000 spectra) is still comparatively small and the number of samples in each class highly imbalanced (see Table I), we used a stratified 5-fold cross-validation approach for training.

Table II shows the results for the classification of SPMS data. Listed are the most common performance metrices, i.e. accuracy, recall and precision, achieved with the proposed 2D-CNN classifier along with two classical 2D-CNN architectures (AlexNet and VGG11) and the previously applied 1D-CNN classifier. All models were tested with the same data.

The confusion matrix in Fig. 4 shows the classification accuracy of the proposed 2D-CNN classification network for each of the 13 classes in the dataset. Iron subclasses (Fe-Sul-Nit, Fe-Nit, Fe-Nit-EC, Fe-dominant) are obviously a bit more difficult to distinguish; all other classes were correctly recognized with rates of > 90%, up to > 98%.

We used padding technique after each convolution to preserve the spatial dimension of feature maps so that the input of the deeper convolutional layers still has a sufficiently large amount of information. Since the size of the spectral images used in this study is relatively small (16×15 pixels), benchmark algorithms designed for high-resolution image data like AlexNet or VGG did not perform well and are not very suitable for the SPMS data, due to their larger convolutional kernels and deeper networks. The size of the first convolutional kernel of AlexNet is 11×11, and the smallest architecture in the VGG family, VGG11, already has 8 convolutional kernel layers. The results also reveal that the classification performance of the proposed 2D-CNN architecture is superior to a 1D-CNN architecture that extracts the information directly from the original mass spectra. Table III indicates the number of trainable parameters in each network. In order to apply AlexNet and VGG to classify the SPMS data, some parameters like the dimension of the input data from the convolutional layer to the first fully connected layer had to be modified. As a result, the modified AlexNet and VGG models have fewer parameters than their original networks.

TABLE II. CLASSIFICATION RESULTS FOR DIFFERENT ALGORITHMS WITH 5-FOLD CROSS VALIDATION ON THE TEST SET, WHERE ALEXNET, VGG11 AND THE PROPOSED 2D-CNN NETWORK HAVE AN INPUT DATA SIZE OF 16×15. THE 1D-CNN NETWORK HAS AN INPUT DATA SIZE OF 1×240.

Method	Overall accuracy	Recall	Precision
AlexNet [19]	87.5 ± 0.5	87.4 ± 0.3	87.1 ± 0.6
VGG11 [20]	90.2 ± 0.3	89.9 ± 0.5	89.9 ± 0.4
1D-CNN [21]	90.4 ± 0.9	89.2 ± 0.2	90.1 ± 0.2
Proposed 2D-CNN	$\mathbf{92.0 \pm 0.1}$	$\mathbf{91.9 \pm 0.1}$	$\mathbf{91.9 \pm 0.1}$

Fig. 4. Normalized confusion matrix displaying the rates (in percent) for the classification of ~7,500 mass spectra with the optimized trained 2D-CNN classifier. On the main diagonal are the percentages of correct predictions for each class, all other entries being incorrect predictions.

TABLE III. NUMBER OF TRAINABLE PARAMETERS FOR DIFFERENT NETWORKS USED FOR SPMS DATA CLASSIFICATION (UNIT: MILLION)

AlexNet [19]	VGG11 [20]	1D-CNN [21]	Proposed 2D-CNN
57.0 M	30.2 M	30.6 M	**2.7 M**

It is also worth noticing that during tuning, the CNNs performed better when using padding to fill the pixels at each edge than without padding. Analyzing the results for the numerous hyperparameters of the grid search tests, we found that downsampling with Max Pooling after each convolutional layer reduces the accuracy. Best results were obtained by applying a 3×3 Max Pooling layer followed by

the ReLU activation function only once, after the last convolutional layer. Besides, we discovered in tests that batch normalization after the last convolutional layer significantly improves the performance of the model, with an accuracy improvement of about 2% compared to the network without batch normalization.

V. CONCLUSION

Rapid chemical profiling of particle matter (PM) is of high interest for many applications, to monitor and document cases of air pollution or to prevent health hazards. The chemical composition of PM can reveal the most likely source of emissions as well as the approximate distance to it. In this study, a comprehensive and flexible approach for reliable automatic classification of aerosols, based on characteristic patterns in the mass spectra from real-time measurements with a single-particle mass spectrometer (SPMS) instrument, was investigated. The classification is based on trained Convolutional Neural Networks (CNN), capable of self-determined automatic learning of detailed characteristic features of those mass spectra. For compact 2D data representation, preferable due to the advantages of 2D convolutions for pattern recognition to extract characteristic local and global features, the 1D mass spectral vectors are converted into 2D matrices and applied to a trained 2D-CNN network. The architecture and hyperparameter values of the CNN network were optimized by a grid search approach. To train the network and test its classification performance, a dataset of ~37,000 labeled mass spectra assigned to one of 13 different aerosol classes was used. As a result, the proposed 2D-CNN architecture outperformed several widely known image processing algorithms based on 2D-CNN approaches as well the 1D-CNN solution proposed recently [21]. For the classification of ~7,500 SPMS spectra, a high mean accuracy of ~92% for the classification of 13 abundant aerosol particle classes was achieved.

This study demonstrates for the first time, that 2D-CNN is highly capable of online classification of aerosol particles analyzed by an SPMS instrument in real-time. For wide-scale and long-term monitoring of aerosol emissions, utilizing a network of several SPMS instruments at different locations, we must face the problem of significant alterations of characteristic features in the data, depending on the location, the wind conditions and seasonal changes at different measurement sites. Future work, therefore, requires to expand and enrich the available datasets of labeled data to obtain more generalized prediction models.

In conclusion, the combination of SPMS measurement techniques with artificial intelligence has unique potential to build comprehensive real-time systems for monitoring the chemical composition of aerosol particles in the atmosphere.

REFERENCES

[1] M. L. Bell, F. Dominici, K. Ebisu, S. L. Zeger, and J. M. Samet, "Spatial and Temporal Variation in PM 2.5 Chemical Composition in the United States for Health Effects Studies," Environ Health Perspect, vol. 115, no. 7, pp. 989–995, Jul. 2007, doi: 10.1289/ehp.9621.

[2] L. Tian et al., "Shipping emissions associated with increased cardiovascular hospitalizations," Atmospheric Environment, vol. 74, pp. 320–325, Aug. 2013, doi: 10.1016/j.atmosenv.2013.04.014.

[3] J. Laskin, A. Laskin, and S. A. Nizkorodov, "Mass Spectrometry Analysis in Atmospheric Chemistry," Anal. Chem., vol. 90, no. 1, pp. 166–189, Jan. 2018, doi: 10.1021/acs.analchem.7b04249.

[4] K. A. Pratt and K. A. Prather, "Mass spectrometry of atmospheric aerosols—Recent developments and applications. Part II: On-line mass spectrometry techniques," Mass Spectrometry Reviews, vol. 31, no. 1, pp. 17–48, 2012, doi: 10.1002/mas.20330.

[5] J. Passig and R. Zimmermann, Laser Ionization in Single-Particle Mass Spectrometry. In Photoionization and Photo-Induced Processes in Mass Spectrometry (eds R. Zimmermann and L. Hanley). Wiley, 2021, Available: https://onlinelibrary.wiley.com/doi/book/10.1002/9783527682201

[6] J. Schade et al., "Spatially Shaped Laser Pulses for the Simultaneous Detection of Polycyclic Aromatic Hydrocarbons as well as Positive and Negative Inorganic Ions in Single Particle Mass Spectrometry," Anal. Chem., vol. 91, no. 15, pp. 10282–10288, Aug. 2019, doi: 10.1021/acs.analchem.9b02477.

[7] J. Passig et al., "Detection of ship plumes from residual fuel operation in emission control areas using single-particle mass spectrometry," Atmos. Meas. Tech., vol. 14, no. 6, pp. 4171–4185, Jun. 2021, doi: 10.5194/amt-14-4171-2021.

[8] A. Zelenyuk, J. Yang, D. Imre, and E. Choi, "Achieving Size Independent Hit-Rate in Single Particle Mass Spectrometry," Aerosol Science and Technology, vol. 43, no. 4, pp. 305–310, Mar. 2009, doi: 10.1080/02786820802637915.

[9] A. Zelenyuk, J. Yang, E. Choi, and D. Imre, "SPLAT II: An Aircraft Compatible, Ultra-Sensitive, High Precision Instrument for In-Situ Characterization of the Size and Composition of Fine and Ultrafine Particles," Aerosol Science and Technology, vol. 43, no. 5, pp. 411–424, Apr. 2009, doi: 10.1080/02786820802709243.

[10] C. J. Gaston et al., "The impact of shipping, agricultural, and urban emissions on single particle chemistry observed aboard the R/V Atlantis during CalNex: SINGLE PARTICLE CHEMISTRY DURING CALNEX," J. Geophys. Res. Atmos., vol. 118, no. 10, pp. 5003–5017, May 2013, doi: 10.1002/jgrd.50427.

[11] J. Arndt et al., "Sources and mixing state of summertime background aerosol in the north-western Mediterranean basin," Atmos. Chem. Phys., vol. 17, no. 11, pp. 6975–7001, Jun. 2017, doi: 10.5194/acp-17-6975-2017.

[12] L. Anders et al., "Detection of ship emissions from distillate fuel operation via single-particle profiling of polycyclic aromatic hydrocarbons," Environ. Sci.: Atmos., vol. 3, no. 8, pp. 1134–1144, 2023, doi: 10.1039/D3EA00056G.

[13] J. Arndt et al., "Characterization and source apportionment of single particles from metalworking activities," Environmental Pollution, vol. 270, p. 116078, Feb. 2021, doi: 10.1016/j.envpol.2020.116078.

[14] R. M. Healy et al., "Source apportionment of PM2.5 in Cork Harbour, Ireland using a combination of single particle mass spectrometry and quantitative semi-continuous measurements," Atmos. Chem. Phys., vol. 10, no. 19, pp. 9593–9613, Oct. 2010, doi: 10.5194/acp-10-9593-2010.

[15] M. Dall'Osto and R. Harrison, "Chemical characterisation of single airborne particles in Athens (Greece) by ATOFMS," Atmospheric Environment, vol. 40, no. 39, pp. 7614–7631, Dec. 2006, doi: 10.1016/j.atmosenv.2006.06.053.

[16] L. Li et al., "Ambient particle characterization by single particle aerosol mass spectrometry in an urban area of Beijing," Atmospheric Environment, vol. 94, pp. 323–331, Sep. 2014, doi: 10.1016/j.atmosenv.2014.03.048.

[17] C. D. Christopoulos, S. Garimella, M. A. Zawadowicz, O. Möhler, and D. J. Cziczo, "A machine learning approach to aerosol classification for single-particle mass spectrometry," Atmos. Meas. Tech., vol. 11, no. 10, pp. 5687–5699, Oct. 2018, doi: 10.5194/amt-11-5687-2018.

[18] G. Wang et al., "Machine learning approaches for automatic classification of single-particle mass spectrometry data," EGUsphere, May 2023, doi: 10.5194/egusphere-2023-784, in press.

[19] A. Krizhevsky, I. Sutskever, and G. E. Hinton, "ImageNet classification with deep convolutional neural networks," Commun. ACM, vol. 60, no. 6, pp. 84–90, May 2017, doi: 10.1145/3065386.

[20] K. Simonyan and A. Zisserman, "Very Deep Convolutional Networks for Large-Scale Image Recognition." arXiv, Apr. 10, 2015. Accessed: Sep. 23, 2023. [Online]. Available: http://arxiv.org/abs/1409.1556

[21] G. Wang et al., "1D-CNN network based real-time aerosol particle classification with single-particle mass spectrometry," IEEE Sens. Lett., pp. 1–4, 2023, doi: 10.1109/LSENS.2023.3315554.

[22] J. Passig et al., "Single-particle characterization of polycyclic aromatic hydrocarbons in background air in northern Europe," Atmospheric Chemistry and Physics, vol. 22, no. 2, pp. 1495–1514, 2022, doi: 10.5194/acp-22-1495-2022.

[23] A. P. Ault, C. J. Gaston, Y. Wang, G. Dominguez, M. H. Thiemens, and K. A. Prather, "Characterization of the Single Particle Mixing State of Individual Ship Plume Events Measured at the Port of Los Angeles," ACS Publications. Accessed: Sep. 29, 2023. [Online]. Available: https://pubs.acs.org/doi/epdf/10.1021/es902985h

[24] R. M. Healy, I. P. O'Connor, S. Hellebust, A. Allanic, J. R. Sodeau, and J. C. Wenger, "Characterisation of single particles from in-port ship emissions," Atmospheric Environment, vol. 43, no. 40, pp. 6408–6414, Dec. 2009, doi: 10.1016/j.atmosenv.2009.07.039.

[25] Q. Xiao et al., "Characteristics of marine shipping emissions at berth: profiles for particulate matter and volatile organic compounds," Atmos. Chem. Phys., vol. 18, no. 13, pp. 9527–9545, Jul. 2018, doi: 10.5194/acp-18-9527-2018.

[26] X. Wang et al., "Atmospheric pollution from ships and its impact on local air quality at a port site in Shanghai," Atmos. Chem. Phys., vol. 19, no. 9, pp. 6315–6330, May 2019, doi: 10.5194/acp-19-6315-2019.